First Direct Evidence of Turbulence-Driven Main Ion Flow Triggering the L-H Transition

L. Schmitz[1], B.A. Grierson[2], L. Zeng[1], T.L. Rhodes[1], J.A. Boedo[3], D. Eldon[3], C. Chrystal[3], G.R. McKee[4], Z. Yan[4], W.A. Peebles[1], G.R.Tynan[3], P.H. Diamond[3], R.J. Groebner[5], K.H. Burrell[5], E.J. Doyle[1]and G. Wang[1]

[1]*University of California, Los Angeles, Los Angeles, CA 90095-7099, USA*
[2]*Princeton Plasma Physics Laboratory, Princeton, New Jersey 08543, USA*
[3]*University of California San Diego, La Jolla, CA 92093, USA*
[4]*University of Wisconsin-Madison, 1500 Engineering Dr., Madison, WI 53706, USA*
[5]*General Atomics, PO Box 85608, San Diego, California 92186-5608, USA*

Simultaneous measurements of main ion flow [via main ion charge exchange recombination (CER) spectroscopy], $\boldsymbol{E}\times\boldsymbol{B}$ flow, and turbulence level $\tilde{n}/n$ [via Doppler backscattering (DBS)] during L-H transitions with extended limit cycle oscillations (LCO) [1], show for the first time that the initial (transient) turbulence collapse preceding the L-H transition is caused by turbulence-generated main ion flow and $\boldsymbol{E}\times\boldsymbol{B}$ *opposing* the equilibrium (L-mode) edge plasma equilibrium $\boldsymbol{E}\times\boldsymbol{B}$ flow related to the edge ion pressure gradient. The formation dynamics of edge transport barriers is crucial for understanding the physics basis of the empirical L-H transition power threshold scaling, and for confidently extrapolating auxiliary heating requirements to burning plasmas. Evidence from several recent experiments has pointed towards a synergistic role of turbulence-driven flows [Zonal Flows (ZFs)] and pressure-gradient-driven flows in the trigger and evolution of the L-H transition [2-6]. L-H transitions preceded by LCO have been obtained in DIII-D near marginal input power P_{th} ($0.75 \leq P/P_{th} \leq 2$) across a range of plasma currents

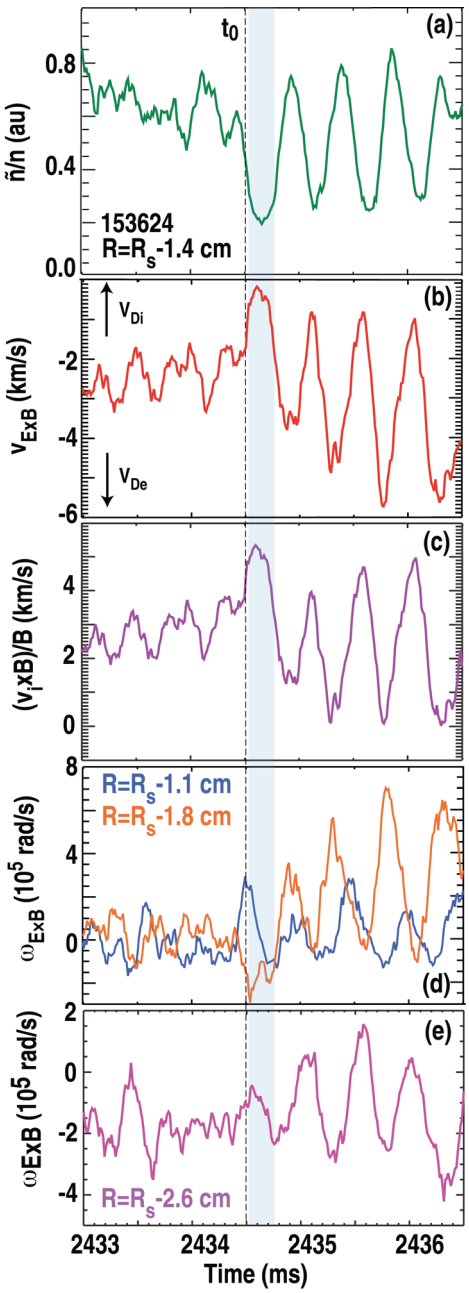

Fig. 1. Time evolution of (a) relative density fluctuation level; (b) $\boldsymbol{E}\times\boldsymbol{B}$ velocity, and (c) main ion $\mathbf{v}_i\times\boldsymbol{B}$ contribution to the $\boldsymbol{E}\times\boldsymbol{B}$ velocity at R=R_s-1.4 cm; (d) shearing rate ω_{ExB} at two radii inside the LCFS in the outer shear layer; (e) shearing rate at R=R_s-2.6 cm in the inner shear layer. The time of initial turbulence suppression is indicated by a grey bar; R_s is the LCFS radius.

($0.6 \le I_p \le 1.5$ MA, edge safety factor ($3.8 \le q_{95} \le 8$), and plasma density ($1\text{x}10^{19}$ m^{-3} $\le \langle n \rangle \le$ $5.5\text{x}10^{19}$ m^{-3}). Figure 1(a,b) shows the time evolution of the density fluctuation level $\tilde{n}$, measured via DBS [7,8] at a normalized wavenumber $k_\theta \rho_s \sim 0.5$, and the total $\boldsymbol{E}\times\boldsymbol{B}$ velocity determined from the Doppler shift of the backscattered signal, in a lower single null (LSN) diverted deuterium plasma (L-mode density $\langle n \rangle = 3\text{x}10^{19}$ m^{-3}, $I_p = 0.75$ MA, B~1.8 T). The data shown in Fig. 1(a-d) is obtained 3 cm above the tokamak midplane, outboard of the minimum in the radial electric field (in the outer $\boldsymbol{E}\times\boldsymbol{B}$ shear layer). The probed radius and the probed poloidal wavenumber are extracted via GENRAY ray tracing, using radial density profiles reconstructed with high time resolution (25 μs) from profile reflectometry. Figure 1(c) shows the $\mathbf{v}_i\times\boldsymbol{B}$ component of the $\boldsymbol{E}\times\boldsymbol{B}$ velocity, calculated from the main ion momentum balance equation $\mathbf{v}_{E\times B} = -1/(Z_i e n_i B)\partial n_i T_i/\partial r + (\mathbf{v}_i \times \boldsymbol{B})/B$ (where Z_i, n_i, T_i, and v_i are the main ion charge number, density, temperature and fluid velocity) by subtracting the pressure gradient term from the total $\boldsymbol{E}\times\boldsymbol{B}$ velocity. ∇P_i is approximated using the electron density from profile reflectometry (as Z_{eff}~1.6 and $n_{iC} << n_i$) and the carbon ion temperature from CER (assuming $T_{iC} \sim T_i$). Fluctuation suppression is first observed in the outer shear layer at $t=t_0$ during a positive peak of the $\mathbf{v}_i\times\boldsymbol{B}$ term [Fig. 1(c)]. A local $\boldsymbol{E}\times\boldsymbol{B}$ flow reversal is also observed at this time [Fig. 1(d)], leading to concomitant large positive and negative shearing rates within a narrow (1 cm) radial region, characteristic of turbulence-driven (mesoscale) flows. Figure 1(e) shows that the (negative) shearing rate in the inner shear layer (inboard of the minimum) does not initially change significantly as fluctuations are first suppressed, but starts oscillating at the LCO frequency and eventually becomes more negative as the LCO evolves. Hence the outer shear layer is initially most significant for fluctuation suppression and initiating the LCO. We show now that the observed positive flow transients are consistent with turbulence-driven poloidal ion flow and $\boldsymbol{E}\times\boldsymbol{B}$ flow, and inconsistent with turbulence suppression via diamagnetic (profile) shear in the early LCO phase.

The cross-correlations between turbulence envelope, main ion flow, and pressure-gradient driven flow, and their detailed spatio-temporal evolution have been measured in a helium plasma with dominant ECH ($\langle n \rangle \sim 3.5\text{x}10^{19}$ m^{-3}, $I_p \sim 0.8$ MA, B=1.8 T). Figure 2 shows that the main ion poloidal flow $v_{i\theta}$ (obtained via main ion CER) lags $\tilde{n}$ after the L-mode-LCO transition and is nearly in phase with $v_{\mathbf{E}\times\mathbf{B}}$. Both results are consistent with dominant turbulence-driven poloidal flow/ZF early during the LCO phase. No corresponding correlation of $\tilde{n}$, and $v_{\mathbf{E}\times\mathbf{B}}$ with the toroidal ion flow is found in the early LCO.

The causality of shear flow generation has been investigated via correlation analysis of the $\boldsymbol{E}\times\boldsymbol{B}$ flow shearing rate, and the ion pressure gradient/diamagnetic flow. Figure 3 shows that the total $\boldsymbol{E}\times\boldsymbol{B}$ shearing rate leads the ion pressure gradient $-\nabla P_i$ early in the LCO, establishing clearly that the $\boldsymbol{E}\times\boldsymbol{B}$ flow shear modulation is not caused by $-\nabla P_i$ changes. Later in the LCO closer to the final H-mode transition ($t_H = t_0$+18 ms), the periodic reduction in edge turbulence and edge transport enables a gradual increase (and periodic modulation) of the edge pressure gradient and ion diamagnetic flow such that $\omega_{\mathbf{E}\times\mathbf{B}}$ then lags $-\nabla P_i$. Figure 4(a-c) show the time evolution of the density gradient (used here as proxy for the ion pressure gradient, the $\boldsymbol{E}\times\boldsymbol{B}$ flow, and the density fluctuation level. It has been confirmed that the ion pressure gradient oscillations are in phase with the density gradient oscillations [9]. An expanded view [Fig. 4(d,e)] shows that $-\nabla P_i$ increases periodically, generating strong negative $\boldsymbol{E}\times\boldsymbol{B}$ flow (blue bar). The data suggest that later in the LCO phase, the turbulence growth rate (and $\tilde{n}$) increase due to the increasing $-\nabla P_i$ within each cycle, in turn driving radial transport and reducing $-\nabla P_i$. The turbulence then collapses due to depletion of turbulence energy [10] as (positive) ZF/poloidal ion flow is driven. Reduced radial transport then allows $-\nabla P_i$ to rise again, transiently maintaining fluctuation suppression via profile shear. During the final phase of the LCO the pressure gradient (diamagnetic flow) dominates the mean flow $\boldsymbol{E}\times\boldsymbol{B}$ shearing rate, which becomes sufficiently large to sustain fluctuation suppression and secure the LCO-H-mode transition.

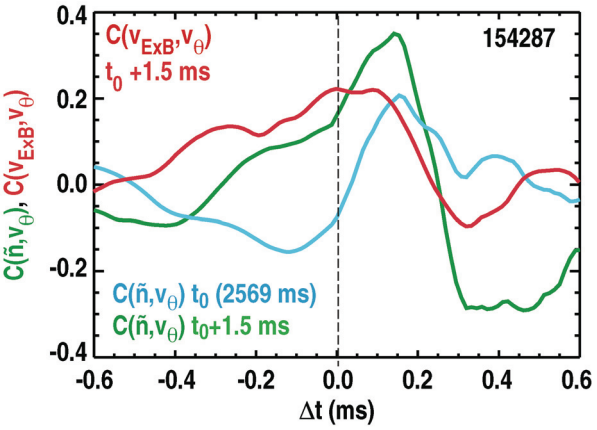

Fig. 2. Cross correlation coefficient of density fluctuation envelope $\tilde{n}$ and poloidal main ion flow velocity $v_{i\theta}$, at the L-LCO transition and 1.5 ms into the LCO phase. The cross correlation of the total $\boldsymbol{E}\times\boldsymbol{B}$ velocity with $v_{i\theta}$, 1.5 ms into the LCO phase, is also shown.

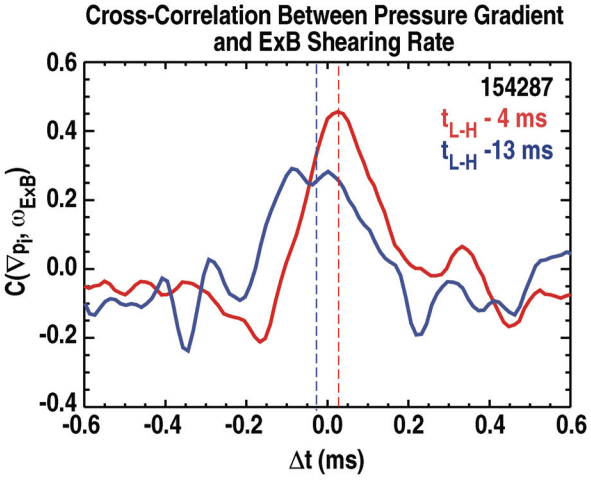

Fig.3: Cross-correlation coefficient between the ion pressure gradient and the $\boldsymbol{E}\times\boldsymbol{B}$ flow shearing rate, about 5 ms after the LCO is triggered ($t_{L\text{-}H}$ – 13 ms) and 4 ms before the final transition to ELM-free H-mode.

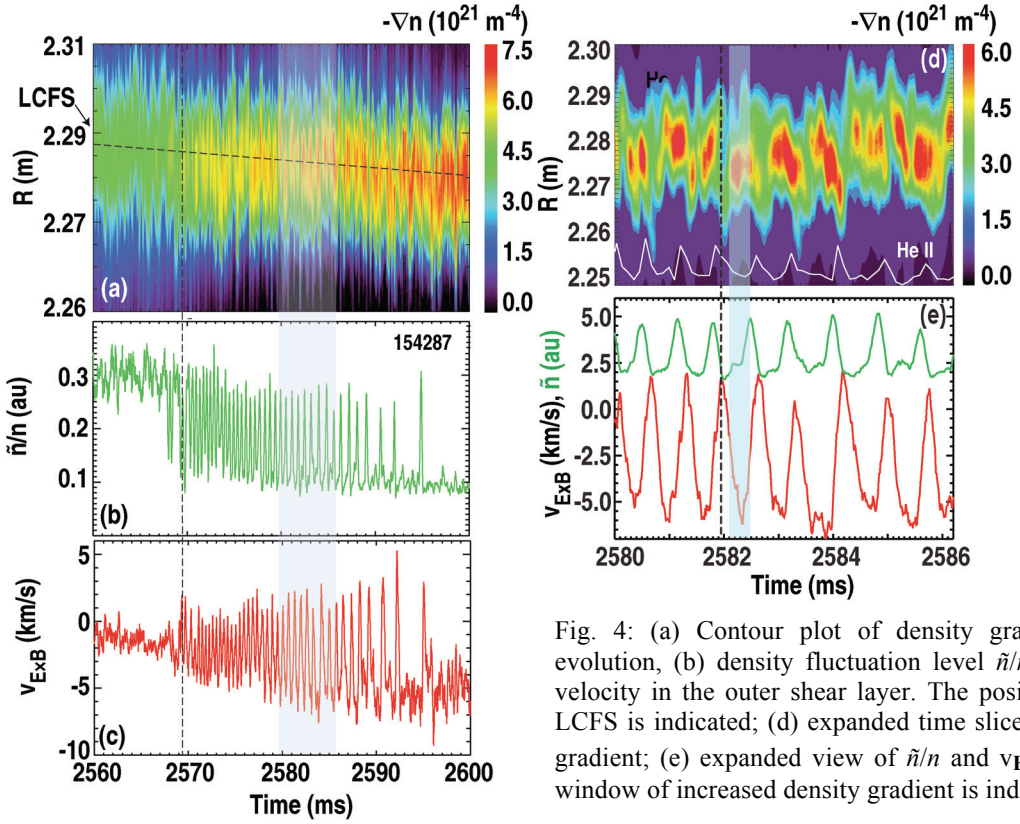

Fig. 4: (a) Contour plot of density gradient time evolution, (b) density fluctuation level $\tilde{n}/n$, (c) $\boldsymbol{E}\times\boldsymbol{B}$ velocity in the outer shear layer. The position of the LCFS is indicated; (d) expanded time slice of density gradient; (e) expanded view of $\tilde{n}/n$ and $v_{\mathbf{E}\times\mathbf{B}}$; a time window of increased density gradient is indicated.

A two-predator, one-prey model, similar to a previously developed model [11,12] but retaining opposite polarity of the turbulence-driven and pressure-gradient-driven $\boldsymbol{E}\times\boldsymbol{B}$ flow, captures essential aspects of the transition dynamics, and is consistent with the direction of the ($\tilde{n}$, E_r) limit cycle observed in the outer shear layer in DIII-D [1], and recently in JFT-2M [13] (increasing $\tilde{n}$ precedes the increase of $\boldsymbol{E}\times\boldsymbol{B}$ flow in the positive [ion diamagnetic] direction). The scaling of the L-LCO transition threshold power and LCO frequency with edge plasma density, collisionality, and q_{95} has been investigated. The initial results indicate that the LCO is triggered at a critical value of turbulence-driven flow shear.

This work was supported by the US Department of Energy under DE-FG02-08ER54984, DE-FG03-01ER54615, DE-AC02-9CH11466, DE-FG02-07ER54917, DE-FG02-89ER53296, DE-FG02-08ER54999, and DE-FC02-04ER54698.

[1] L. Schmitz, L. Zeng, T.L. Rhodes, et al., Phys. Rev. Lett. **108**, 155002-5 (2012).
[2] G.R. McKee et al., Nucl. Fusion **49**, 115016 (2009).
[3] S.J. Zweben, R.J.Maqueda, R. Hager, et al., Phys. Plasmas **17**, 102502 (2010).
[4] G.D. Conway, C. Angioni, F. Ryter, et al., Phys. Rev. Lett. **106**, 065001 (2011).
[5] G.S. Xu et al., Phys. Rev. Lett. **107**, 125001 (2011).
[6] T. Estrada, C. Hidalgo, T. Happel, et al., Phys. Rev. Lett. **107**, 245004 (2011).
[7] W.A.Peebles, T.L. Rhodes, J.C. Hillesheim, et al., Rev. Sci. Instrum. **81**, 10D902 (2010).
[8] J.C. Hillesheim et al., Rev. Sci. Instrum. **81**, 10D907 (2010).
[9] L. Schmitz et al., Nucl. Fusion **54** 073012 (2014).
[10] G. Tynan, et al. Nucl. Fusion **53** 073053 (2012).
[11] E.J. Kim and P.H. Diamond, Phys. Rev. Lett. **90**, 185006 (2003).
[12] K. Miki and P.H. Diamond, Phys. Plasmas **19**, 092306 (2012).
[13] T. Kobayashi, et al., Phys. Rev. Lett. **111**, 035002 (2013).